Available online at www.sciencedirect.com
SCIENCE DIRECT®
Journal of Sound and Vibration 275 (2004) 299–316
JOURNAL OF SOUND AND VIBRATION
www.elsevier.com/locate/jsvi

A purely directional wave splitting for the homogeneous Timoshenko beam

M. Johansson*

Department of Applied Mechanics, Chalmers University of Technology, SE-412 96 Göteborg, Sweden

Received 3 March 2003; accepted 17 June 2003

Abstract

A new wave splitting for the Timoshenko beam is derived, which partially remedies earlier problems with exponentially growing split fields and integral operator kernels. This allows for propagation of the split fields further along the beam and for longer time intervals. The elements of the transform and Green's operator are derived in the Laplace domain and are computed by means of short and long time asymptotic expansions and contour integration. Numerical results are presented for the case of forced motion of the end of a semi-infinite beam and the cases of a point force and a point moment on an infinite beam.
© 2003 Elsevier Ltd. All rights reserved.

1. Introduction

The wave splitting technique has been used extensively in electrodynamic problems to solve direct and inverse scattering problems for various types of media. In a homogeneous one-dimensional domain the electromagnetic waves satisfy a second order wave equation. It can be transformed to yield a system of two first order one-way wave equations, the wave splitting transformation, where the new dependent variables are the split fields. (Alternatively, starting from the first order Maxwell's equations, first order one-way equations may be obtained, e.g., by forming linear combinations.) The wave splitting can be applied to an inhomogeneous one-dimensional domain, usually leading to a coupled system of equations, whereupon various time-domain techniques can be utilized to solve scattering problems. Examples of these methods are the imbedding method, Green's function technique and the wave propagator method. Three examples from a vast number of articles on these methods are [1–3]. These techniques carry over directly to low order mechanical elements such as the string or the rod.

*Tel.: +46-31-772-1524; fax: +46-31-772-3827.
E-mail address: martin.johansson@me.chalmers.se (M. Johansson).

0022-460X/$ - see front matter © 2003 Elsevier Ltd. All rights reserved.
doi:10.1016/j.jsv.2003.06.024

Turning to higher order mechanical waveguides, a common mathematical model for the beam is the Timoshenko equation. It may be written as a fourth order hyperbolic PDE or, alternatively, as a coupled system of first order equations in the spatial co-ordinate, with four dependent variables. A wave splitting for the Timoshenko beam was presented in Ref. [4]. It is obtained by diagonalizing the original system of first order equations. When the wave splitting transform is applied to the dependent variables of the original system of equations, these are transformed into four new dependent variables, the split fields, which are governed by a system of four decoupled first order one-way wave equations. In each direction two different fields propagate with different wave front speeds, the rod velocity and the effective shear velocity. When added, they form the mean transverse deflection field propagating in that direction, while as individual wave fields they have no obvious physical interpretation. This will hereafter be referred to as the original wave splitting. If the original wave splitting is applied to an inhomogeneous beam, the split fields are governed by a coupled system of one-way wave equations. In this context inhomogeneous means that a geometrical or material parameter of the beam varies with the spatial co-ordinate along the beam axis. Time-domain techniques can then be used to solve scattering problems for the beam. Although several scattering problems have been solved [5–8] this method has the undesirable features of split fields and kernels that are exponentially growing. The exponential behaviour is cancelled out when the fields are transformed back to the physical variables, but the applications of the time-domain techniques mentioned above deal with the split fields. With the numerical problems that follow, these features drastically limit the ability to propagate boundary data along the beam as well as the ability to obtain enough boundary data for large inhomogeneous regions. The final goal, to solve an inverse problem, is then confined to determination of moderately distributed inhomogeneities close to the measuring point.

A qualitative understanding of the exponentially growing behaviour is gained from the following argument. For the set of every combination of permissible physical fields, to which the boundary conditions belong, the two split fields travelling in the same direction must coexist. They are, however, treated mathematically as independent. To excite only one of the split fields would require the injection of an unbounded amount of energy into the beam, see Ref. [9]. Hence, each split field behaves as if it carries an unbounded amount of energy, which is manifested in exponential growth. In Refs. [8–11] the authors compensate for the exponential growth by extracting an exponential factor from the split fields, but this merely postpones the problem of taking the difference of two exponentially large fields.

This paper deals with finding a wave splitting for the Timoshenko beam that leads to well behaved split fields and integral operator kernels. The original splitting is the only wave splitting that gives two decoupled wave fields for each direction. This is however done at the price of getting unphysical split fields. By relaxing the condition that the two split fields propagating in the same direction must be decoupled, the unphysical behaviour leading to numerical difficulties can be avoided for the new wave splitting. The mean transverse deflection field may be decomposed into its left and right propagating components. This is a purely directional decomposition into physical wave fields, which are decoupled for homogeneous regions. It corresponds to the factorization of the fourth order Timoshenko equation into two second order PDEs, each governing the propagation in one direction. From here, the split fields of the original wave splitting could be obtained, but instead it is preferable to work with the left and right moving components of the mean transverse deflection and their spatial derivatives. For each direction the

new split fields are coupled, but in contrast to the original wave splitting, this decomposition has the advantage of being physically permissible since there may be coupled waves propagating in only one direction. Moreover, these components are physical wave fields themselves and thereby well behaved. As all transform and propagation operators operate on physical fields it is expected that their kernels are well behaved too. The matter of transforming to the new split fields, as well as propagating them, should then be a question of choosing suitable numerical integration schemes.

After an outline of the Timoshenko equation in Section 2, the new wave splitting transformation is derived in Section 3. In Section 4 Green's function operators for the homogeneous beam are derived. The wave splitting is applied to three different boundary conditions and boundary data are propagated along the beam by means of Green's operators. Numerical results are presented in Section 5. Finally, some concluding remarks are found in Section 6.

2. The Timoshenko beam equation

The Timoshenko beam equation for an homogeneous infinite beam may be written as

$$\partial_x \gamma = c_1^{-2} \partial_t^2 w, \tag{1}$$

$$\partial_x^2 \psi - \frac{f_1}{f_2} \gamma = c_2^{-2} \partial_t^2 \psi, \tag{2}$$

$$\gamma = \partial_x w + \psi, \tag{3}$$

where $w(x,t)$, $\psi(x,t)$ and $\gamma(x,t)$ are the mean transverse deflection, the mean rotation and the mean shear angle of the cross-section, respectively. Note that ψ is defined in a direction opposite to that in Refs. [4,9,12], see Fig. 1. The velocities c_1 (effective shear velocity) and c_2 (rod velocity) are defined by

$$c_1 = \sqrt{k'G/\rho}, \quad c_2 = \sqrt{E/\rho}, \tag{4}$$

and the f_i are the stiffnesses given by

$$f_1 = k'GA, \quad f_2 = EI, \tag{5}$$

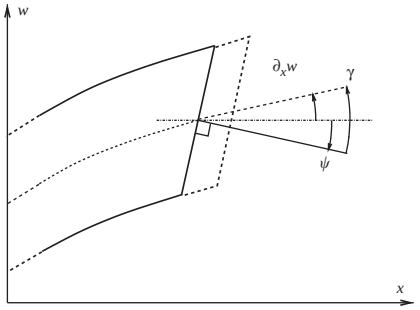

Fig. 1. Geometry of the beam.

where A is the cross-section area, I its moment of inertia and ρ is the density of the beam. E is the modulus of elasticity, G is the shear modulus and k' is the shear coefficient.

The other familiar form of the Timoshenko beam equation is

$$(\partial_x^4 - (c_1^{-2} + c_2^{-2})\partial_x^2\partial_t^2 + r_0^{-2}c_2^{-2}\partial_t^2 + c_1^{-2}c_2^{-2}\partial_t^4)w = 0, \tag{6}$$

where r_0 is the radius of gyration given by $r_0 = \sqrt{I/A}$. Non-dimensional variables are introduced according to

$$x' = x/r_0, \quad t' = t/\tau, \quad w' = w/r_0, \quad \tau = r_0/c_2(q-1), \tag{7}$$

where τ is a characteristic time and q is a non-dimensional parameter given by

$$q = (c_2^2 + c_1^2)/(c_2^2 - c_1^2). \tag{8}$$

For most materials $q > 1$ and $\tau > 0$, see Ref. [4]. Eq. (6) now becomes

$$(\partial_{x'}^4 - 2q(q-1)\partial_{x'}^2\partial_{t'}^2 + (q-1)^2\partial_{t'}^2 + (q^2-1)(q-1)^2\partial_{t'}^4)w' = 0. \tag{9}$$

From hereon, unprimed variables will denote non-dimensional variables unless otherwise stated. This fourth order differential equation can be factorized and written in terms of the eigenoperators defined in Ref. [4]

$$(\partial_x - \lambda_1)(\partial_x + \lambda_1)(\partial_x - \lambda_2)(\partial_x + \lambda_2)w = 0, \tag{10}$$

so that w may be written as the sum

$$w = w_1^+ + w_1^- + w_2^+ + w_2^-, \tag{11}$$

where the $w_i^\pm$ satisfy

$$(\partial_x \pm \lambda_i)w_i^\pm = 0, \quad i = 1, 2. \tag{12}$$

In the Laplace domain the eigenoperators are given by

$$\tilde{\lambda}_i = \sqrt{q-1}\sqrt{qs^2 \pm s\sqrt{s^2-1}}, \quad i = 1, 2. \tag{13}$$

Here, the upper sign refers to $i = 1$ and the lower sign refers to $i = 2$. Some early remarks about these operators can be made here. Their leading terms for large s are $\alpha_1^{-1}s$ and $\alpha_2^{-1}s$, respectively, indicating that they carry a differential operator. The α_i are related to the wave front speeds and are given by

$$\alpha_1^{-1} = \sqrt{q^2-1}, \quad \alpha_2^{-1} = (q-1). \tag{14}$$

The $\tilde{\lambda}_i$ both have branch points in the complex s-plane at $s = \pm 1$. This indicates that they grow exponentially in the time domain. Both also have a branch point at $s = 0$ and $\tilde{\lambda}_2$ has additional branch points at $s = \pm i\alpha_1$, which indicates an oscillatory behaviour in the time domain. The eigenoperators are thus built up by a differential operator and a convolution with an exponentially growing kernel. This feature also appears in the transformation operator matrices that transform between the physical and the split fields when the original wave splitting is used. For a more extensive discussion of these operators, see Refs. [4,9].

3. Decomposition into waves travelling in different directions

The original wave splitting transforms from the physical variables to $w_i^{\pm}$, $i = 1, 2$. Thus, in addition to decomposing the wave field into parts travelling in opposite directions, it also transforms into wave fields satisfying decoupled first order one-way equations. By removing the decoupling operation, a purely directional wave splitting is obtained. As will be seen, it also removes the problem of exponentially growing split fields and kernels. To achieve this it is sufficient to factorize the homogeneous Timoshenko equation into the product of two second order one-way differential operators, thus retaining the coupling between the waves propagating in the same direction albeit with different wave front speeds. This is readily done by inspection of Eq. (10). The new PDEs are

$$\partial_x^2 w^{\pm} \pm \mathscr{A}\partial_x w^{\pm} + \mathscr{B} w^{\pm} = 0, \quad w = w^{+} + w^{-}, \tag{15}$$

where, $\mathscr{A} = \lambda_1 + \lambda_2$ and $\mathscr{B} = \lambda_1\lambda_2$. The new split fields, $w^{\pm}$, where w^{+} is the part of w that propagates in the positive x direction and w^{-} is the part propagating in the negative x direction, may exist independently of each other and satisfy the same conditions as w. They are therefore not exponentially growing (unless the forcing is). Moreover, they are related to the split fields of the original wave splitting as $w^{\pm} = w_1^{\pm} + w_2^{\pm}$. The dynamics for the new split fields are

$$\partial_x \mathbf{w} = \begin{pmatrix} 0 & 1 & 0 & 0 \\ -\mathscr{B} & -\mathscr{A} & 0 & 0 \\ 0 & 0 & 0 & 1 \\ 0 & 0 & -\mathscr{B} & \mathscr{A} \end{pmatrix} \mathbf{w}, \quad \mathbf{w} = \begin{pmatrix} w^{+} \\ \partial_x w^{+} \\ w^{-} \\ \partial_x w^{-} \end{pmatrix}. \tag{16}$$

To obtain the wave splitting transformation, relations between the physical fields and the split fields are sought. Here, it is convenient to choose the physical field vector as $\mathbf{u} = (w, \partial_x w, \psi, \partial_x \psi)^{\mathrm{T}}$. If γ is desired, it is easily obtained by means of Eq. (3). From the second member of Eq. (15), relations for w and $\partial_x w$ are obtained. Since the split fields are truly independent for the homogeneous beam, so are the corresponding rotation angles, $\psi^{\pm}$. Hence, the ansatz

$$\psi^{\pm} = \mathscr{C}^{\pm} w^{\pm} + \mathscr{D}^{\pm}\partial_x w^{\pm}, \quad \psi = \psi^{+} + \psi^{-}, \tag{17}$$

is made. The operators $\mathscr{C}^{\pm}$ and $\mathscr{D}^{\pm}$ are only time dependent. Insertion into the non-dimensional version of Eq. (1) using Eq. (3) gives

$$\partial_x^2 w^{\pm} + (1 + \mathscr{D}^{\pm})^{-1}\mathscr{C}^{\pm}\partial_x w^{\pm} - (1 + \mathscr{D}^{\pm})^{-1}\alpha_1^{-2}\partial_t^2 w^{\pm} = 0. \tag{18}$$

By identifying terms of Eqs. (15) and (18) the operators are obtained as

$$\begin{aligned} \mathscr{D}^{\pm} &= \mathscr{D} = -1 - \alpha_1^{-2}\partial_t^2\mathscr{B}^{-1}, \\ \mathscr{C}^{\pm} &= \pm\mathscr{C} = \pm(-\alpha_1^{-2}\partial_t^2\mathscr{B}^{-1}\mathscr{A}). \end{aligned} \tag{19}$$

To derive a relation between the spatial partial derivative of the rotation angle and the split fields, Eq. (15) is inserted into the non-dimensional version of Eq. (1) using Eq. (3), giving

$$\partial_x \psi^{\pm} = \alpha_1^{-2}\partial_t^2 w^{\pm} \pm \mathscr{A}\partial_x w^{\pm} + \mathscr{B} w^{\pm}. \tag{20}$$

Denoting the wave splitting transformation operator by $\mathbf{P}$, Eqs. (15), (17) and (20) now define the inverse transformation, from the split fields, $\mathbf{w}$, to the physical fields, $\mathbf{u}$.

$$\mathbf{u} = \mathbf{P}^{-1}\mathbf{w} = \begin{pmatrix} 1 & 0 & 1 & 0 \\ 0 & 1 & 0 & 1 \\ \mathscr{C} & \mathscr{D} & -\mathscr{C} & \mathscr{D} \\ (\alpha_1^{-2}\partial_t^2 + \mathscr{B}) & \mathscr{A} & (\alpha_1^{-2}\partial_t^2 + \mathscr{B}) & -\mathscr{A} \end{pmatrix} \mathbf{w}. \tag{21}$$

The forward transformation is

$$\mathbf{w} = \mathbf{P}\mathbf{u} = \frac{1}{2}\begin{pmatrix} 1 & -\mathscr{D}\mathscr{C}^{-1} & \mathscr{C}^{-1} & 0 \\ -(\alpha_1^{-2}\partial_t^2 + \mathscr{B})\mathscr{A}^{-1} & 1 & 0 & \mathscr{A}^{-1} \\ 1 & \mathscr{D}\mathscr{C}^{-1} & -\mathscr{C}^{-1} & 0 \\ (\alpha_1^{-2}\partial_t^2 + \mathscr{B})\mathscr{A}^{-1} & 1 & 0 & -\mathscr{A}^{-1} \end{pmatrix} \mathbf{u}. \tag{22}$$

3.1. Time-domain representations

In the time domain all operators and transform matrix elements are of the form

$$\begin{aligned} \mathscr{F}u &= \sum_{\mu} k_{\mu,\mathscr{F}}\partial_t^{\mu}u + K_{\mathscr{F}} * u \\ &= \sum_{\mu} k_{\mu,\mathscr{F}}\partial_t^{\mu}u + \int_0^t K_{\mathscr{F}}(t')u(t-t')\,\mathrm{d}t', \end{aligned} \tag{23}$$

where $\mu = 0, 1, 2$, and $K_{\mathscr{F}}$ is some kernel function containing, at most, jump discontinuities. The Laplace transformed operators $\tilde{\mathscr{A}}$ and $\tilde{\mathscr{B}}$ are obtained from identification of the product of the Laplace transformed differential operators in Eq. (15) with the Laplace transform of Eq. (9) and are given by

$$\begin{aligned} &\tilde{\mathscr{B}} = \alpha_2^{-2}s(1 + \alpha_1^{-2}s^2)^{1/2}, \\ &\tilde{\mathscr{A}} = (2\tilde{\mathscr{B}} + 2q(q-1)s^2)^{1/2} = (2\alpha_2^{-1}s)^{1/2}((1 + \alpha_1^{-2}s^2)^{1/2} + qs)^{1/2}. \end{aligned} \tag{24}$$

Alternatively, Eq. (13) may be used. $\tilde{\mathscr{A}}$ and $\tilde{\mathscr{B}}$ are both seen to have branch points at $s = \pm \mathrm{i}\alpha_1$. The branch cut is chosen to go between these points along the imaginary axis so that $\mathrm{Re}(1 + \alpha_1^{-2}s^2)^{1/2}$ and $\mathrm{Re}\, s$ have the same sign. $\tilde{\mathscr{A}}$ also has one additional branch point at $s = 0$. The reason why the branch points at $s = \pm 1$ are absent is due to the fact that both $\tilde{\mathscr{A}}$ and $\tilde{\mathscr{B}}$ are homogeneous polynomials in $\tilde{\lambda}_1$ and $\tilde{\lambda}_2$. Passing through a presumed branch cut emanating from $s = \pm 1$ just changes the subindices of $\tilde{\lambda}_i$ from 1 to 2 and vice versa. The operators thus have the same values on both sides of the cut so no cut is necessary. The case is the same for the Laplace transform of all operators figuring in the wave splitting operators in Eqs. (21) and (22). Then, the Bromwich contour for their inverse Laplace transformation can be placed immediately to the right of the imaginary axis and, as expected, the kernels do not have exponentially growing behaviour.

For $\mathscr{B}$ and $\mathscr{D}$ explicit time domain expressions are given by Eq. (23) with

$$k_{2,\mathscr{B}} = \alpha_2^{-1}\alpha_1^{-1}, \quad k_{0,\mathscr{B}} = \alpha_2^{-1}\alpha_1, \quad K_{\mathscr{B}} = \alpha_1 t^{-1} \mathrm{J}_2(\alpha_1 t),$$
$$k_{0,\mathscr{D}} = -1 - \alpha_1^{-1}\alpha_2, \quad K_{\mathscr{D}} = -\alpha_1 \mathrm{J}_1(\alpha_1 t), \quad k_{1,\mathscr{B}} = k_{2,\mathscr{D}} = k_{1,\mathscr{D}} = 0, \tag{25}$$

where J_n are Bessel functions of order n. The other operators were obtained by the approximate methods described for $\mathscr{A}$ in Appendix A. In Ref. [4], various series representations are obtained for the eigenoperators, λ_i, which are related to the operators presented here. Comments on these are found in Appendix C. Further discussion of the wave splitting transform is found in Section 6.

4. Green's operator matrices for the split fields in homogeneous regions

The main concern in this paper is to be able to propagate the wave fields over long distances and for long times without having problems with large cancellations and exponential behaviour. It is assumed that the wave fields at $x = 0$ are given and propagated to position x. Green's operators can be obtained by solving Eq. (15) in the Laplace domain with $\tilde{w}^{\pm}(0,s)$ and $\partial_x \tilde{w}^{\pm}(0,s)$ known. The split fields, $\tilde{\mathbf{w}}^{\pm}(x,s) = (\tilde{w}^{\pm}(x,s), \partial_x \tilde{w}^{\pm}(x,s))^{\mathrm{T}}$, may then be given in terms of the boundary values as

$$\tilde{\mathbf{w}}^{\pm}(x,s) = \tilde{\mathbf{G}}^{\pm}(x,s)\tilde{\mathbf{w}}^{\pm}(0,s), \quad \tilde{\mathbf{w}}^{\pm}(0,s) = \tilde{\mathbf{G}}^{\pm}(-x,s)\tilde{\mathbf{w}}^{\pm}(x,s), \tag{26}$$

where

$$\tilde{\mathbf{G}}^{+}(x,s) = (\tilde{\lambda}_2 - \tilde{\lambda}_1)^{-1} \begin{pmatrix} \tilde{\lambda}_2 \mathrm{e}^{-x\tilde{\lambda}_1} - \tilde{\lambda}_1 \mathrm{e}^{-x\tilde{\lambda}_2} & \mathrm{e}^{-x\tilde{\lambda}_1} - \mathrm{e}^{-x\tilde{\lambda}_2} \\ -\tilde{\lambda}_1\tilde{\lambda}_2(\mathrm{e}^{-x\tilde{\lambda}_1} - \mathrm{e}^{-x\tilde{\lambda}_2}) & -\tilde{\lambda}_1 \mathrm{e}^{-x\tilde{\lambda}_1} + \tilde{\lambda}_2 \mathrm{e}^{-x\tilde{\lambda}_2} \end{pmatrix}, \tag{27}$$

$$\tilde{\mathbf{G}}^{-}(x,s) = (\tilde{\lambda}_2 - \tilde{\lambda}_1)^{-1} \begin{pmatrix} \tilde{\lambda}_2 \mathrm{e}^{x\tilde{\lambda}_1} - \tilde{\lambda}_1 \mathrm{e}^{x\tilde{\lambda}_2} & -\mathrm{e}^{x\tilde{\lambda}_1} + \mathrm{e}^{x\tilde{\lambda}_2} \\ \tilde{\lambda}_1\tilde{\lambda}_2(\mathrm{e}^{x\tilde{\lambda}_1} - \mathrm{e}^{x\tilde{\lambda}_2}) & -\tilde{\lambda}_1 \mathrm{e}^{x\tilde{\lambda}_1} + \tilde{\lambda}_2 \mathrm{e}^{x\tilde{\lambda}_2} \end{pmatrix}. \tag{28}$$

In the time domain, the elements of Green's operator matrices are convolution operators with kernels that may contain distributions. These can be determined by studying asymptotic expansions of Green's operator elements in the Laplace domain for large s. The elements are built up by expressions like

$$f(\tilde{\lambda}_1, \tilde{\lambda}_2)\mathrm{e}^{\pm x\tilde{\lambda}_i} = [f(\tilde{\lambda}_1, \tilde{\lambda}_2)\mathrm{e}^{\pm x(\tilde{\lambda}_i - s/\alpha_i)}][\mathrm{e}^{\pm xs/\alpha_i}]. \tag{29}$$

The second bracketed factor gives the translation in time of the arrival of the wave front and the first bracketed factor is expressible as an infinite series in inverse powers of s. The leading terms of this series, for each of the elements in Eqs. (27) and (28), gives the coefficients for the distributions.

In that way Green's operator matrix elements can be divided into

$$
\begin{aligned}
G_{11}^{+}(x,t) &= \frac{1}{\alpha_2-\alpha_1}(-\alpha_1\delta(t-x/\alpha_1)+\alpha_2\delta(t-x/\alpha_2))+G_{11}^{K+}(x,t),\\
G_{12}^{+}(x,t) &= G_{12}^{K+}(x,t),\\
G_{21}^{+}(x,t) &= \frac{x}{4\alpha_2(\alpha_2-\alpha_1)}(\alpha_1\delta(t-x/\alpha_1)-\alpha_2\delta(t-x/\alpha_2))\\
&\quad+\frac{1}{\alpha_2-\alpha_1}(\delta'(t-x/\alpha_1)-\delta'(t-x/\alpha_2))+G_{21}^{K+}(x,t),\\
G_{22}^{+}(x,t) &= \frac{1}{\alpha_2-\alpha_1}(\alpha_2\delta(t-x/\alpha_1)-\alpha_1\delta(t-x/\alpha_2))+G_{22}^{K+}(x,t),
\end{aligned}
\tag{30}
$$

where $G_{ij}^{K+}(x,t)$, $i,j=1,2$, are kernel functions that contains, at most, jump discontinuities. The elements of $\mathbf{G}^{-}(x,t)$ can be obtained in the same way but in that case the time translation is in the other direction.

4.1. The inverse Laplace transformation of Green's operator kernels

The aforementioned techniques to perform inverse Laplace transformation, see Appendix A, apply to the Green's operator kernels for small distances x. The long time representation works only after the arrival of the slower wave front, propagating with the velocity c_1. (All kernels contain jump discontinuities at that time.) It depends then on the time range for the short time representation versus the length of time interval between the arrivals of the faster and the slower wave fronts if the approximations overlap. If x is large enough there is an interval where neither of the representations are satisfactory.

In these cases the values of Green's operator kernels must be obtained in another way. One alternative is to perform the contour integration numerically. A similar computation is performed in Ref. [13] and is followed quite closely here. The integrals are of the form

$$
(2\pi\mathrm{i})^{-1}\int_{Br} f(\tilde{\lambda}_1,\tilde{\lambda}_2)\mathrm{e}^{\tilde{h}(s)}\,\mathrm{d}s, \tag{31}
$$

where $f(\tilde{\lambda}_1,\tilde{\lambda}_2)$ is a rational function of the eigenoperators and the $\tilde{h}(s)$ are given in Table 1. Since all integrals contains both of $\tilde{\lambda}_i$, and thus have branch points at $s=0,\pm1,\pm\mathrm{i}\alpha_1$, the contours are taken according to Fig. 2.

For some elements and large s, the integrands $f(\tilde{\lambda}_1,\tilde{\lambda}_2)$ have leading terms of order s or 1. In these cases the leading terms are extracted and treated separately since they have exact inverse Laplace transforms, see Eq. (30). The remaining part of the integrals along the arcs C_1 and C_2 can then be shown to give a zero result by Jordan's lemma. Moreover, since the exponential order of the integrands depends on the different $\tilde{h}(s)$, the contour integrations are performed to the left or

Table 1
Contour choices for different exponents

$\tilde{h}(s)$	C_{right}	C_{left}
$st\pm x\tilde{\lambda}_i$	$\alpha_i t<\mp x$	$\alpha_i t>\mp x$

right of the original contour for different values of the time variable. These are given in Table 1. When the integrals can be taken along C_{right} they give a zero result. Along each contour the integrals are rewritten as integrals of a real variable, for details see [13–15]. The only integrals that contribute to the total integral are those along L_2 through L_9. The sum of integrals along the C_{left} are given in Table 2, in which the integrals I_1 through I_{12} are found in Appendix B. The asymptotic expansions of the kernels in Table 2 for large values of t, calculated according to Appendix A, show that there is no contribution from the branch points $s = \pm 1$. Hence, they are not exponentially growing. The numerical results confirm this.

5. Numerical examples

In this section numerical results from the wave splitting and the propagation with Green's operator matrix are presented. The convolution integrals were computed by means of the trapezoidal rule and the differentiations were approximated by numerical differentiation with the

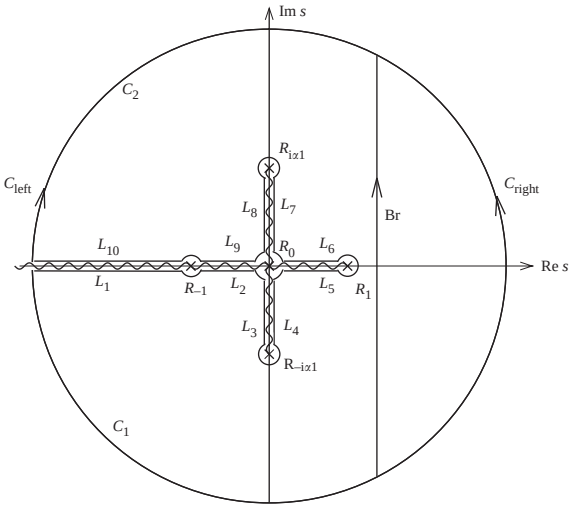

Fig. 2. Integration contours for Green's operator kernels.

Table 2
The integrals of Green's function kernels

Kernel	$t < x/\alpha_2$	$x/\alpha_2 < t < x/\alpha_1$	$t > x/\alpha_1$
$G_{11}^{K+}(x,t)$	0	$I_1 + I_2$	$I_1 + I_3$
$G_{12}^{K+}(x,t)$	0	$I_4 + I_5$	$I_4 + I_6$
$G_{21}^{K+}(x,t)$	0	$I_7 + I_8$	$I_7 + I_9$
$G_{22}^{K+}(x,t)$	0	$I_{10} + I_{11}$	$I_{10} + I_{12}$

central point rule (with some modifications at $t = 0$). The responses for three different boundary conditions are presented. The first, is one of the boundary conditions from Refs. [9,13], which is

$$\text{BC1: } \begin{cases} \partial_x \psi(0,t) = 0, \\ w(0,t) = v_0 t_1 \mathrm{H}(t_1), \end{cases} \tag{32}$$

where $t_1 = \alpha_2 t$, v_0 is a non-dimensional constant and $\mathrm{H}(t_1)$ is the Heaviside function. This boundary condition represents forced motion of the free end of a semi-infinite beam. The responses are shown in Fig. 3. The second and third boundary conditions are

$$\text{BC2: } \begin{cases} \psi(0,t) = 0, \\ Q(0,t) = Q_0 f(t) \end{cases} \quad \text{and} \quad \text{BC3: } \begin{cases} w(0,t) = 0, \\ M(0,t) = M_0 f(t), \end{cases} \tag{33}$$

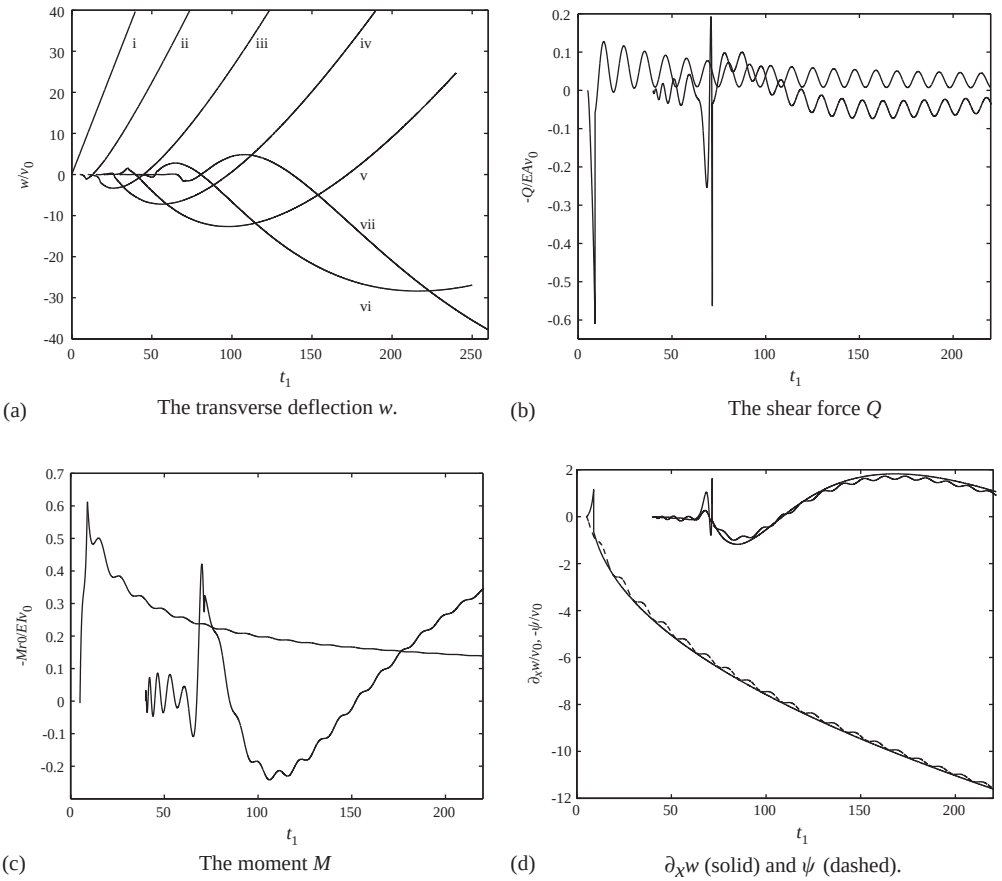

(a) The transverse deflection w. (b) The shear force Q.

(c) The moment M. (d) $\partial_x w$ (solid) and ψ (dashed).

Fig. 3. The responses for BC1 at various positions x. (a) i–vii: positions $x = 0, 5, 10, 15, 20, 30, 40$, respectively, (b–d): positions $x = 5$ and 40.

where Q_0 and M_0 are constant force and moment magnitudes, respectively, and

$$f(t) = \begin{cases} \sin^2(\omega_0 t/2), & t \in (0, 2\pi/\omega_0), \\ 0, & t \notin (0, 2\pi/\omega_0). \end{cases} \tag{34}$$

The boundary condition BC2 represents a time-dependent point force of magnitude $2Q_0 f(t)$ at $x = 0$ on an infinite beam, while BC3 represents a time-dependent bending point moment of magnitude $2M_0 f(t)$. The responses are shown in Figs. 4 and 5. The scaling of the time variable t_1 is the one used in Refs. [9,13] and makes the first and second wave fronts arrive at a given position x at times $t_1 = x$ and $t_1 = \alpha_2/\alpha_1 x$ respectively. In all examples the numerical values $q = 21/11$, $\alpha_1 = 11/8\sqrt{5}$, $\alpha_2 = 11/10$, $v = 0.3$ and $k' = 0.813$, have been used.

Figs. 3(a) and (b) show the mean transverse deflection and the shear force respectively. If the interval $t \in (0, 20)$ is zoomed in, it is clearly visible that the response at $x = 5$ is in agreement with the results of Ref. [9]. The corresponding response for the moment in Fig. 3(c) differs by a scaling factor which is believed to be due to a scaling error in Ref. [9]. Some features in Figs. 3(a)–(d) are worthy of notice. The oscillations that mark out the responses of the shear force, the moment and the rotation angle form the response from the lowest thickness-shear mode. In the dimensionless time-scale t, α_1 is the cut-off frequency for this mode, corresponding to the imaginary roots of $\tilde{\lambda}_2$. In the interval before the arrival of the slower wave front, the disturbances have propagated with group velocities which are higher than the effective shear velocity. Taking into consideration the dispersion relation for the Timoshenko beam, this is part of the response from the second branch, the thickness-shear mode, more specifically the part for which the group velocity of the second branch is higher than the effective shear velocity. There is thus a non-dimensional threshold frequency, $\alpha_3 (> \alpha_1)$, below which the corresponding disturbances do not propagate faster than the slower wave front. As t increases the dominating frequency of the oscillating motion approaches the cut-off frequency. This is illustrated most clearly in Figs. 3(a) and (c).

The jump discontinuities in the shear force, Fig. 3(b), in fact have the same magnitude at both positions, $x = 5$ and 40, something that is not evident from the graph due to the resolution. In the computation of the moment for BC1, the numerical differentiation breaks down at the arrival

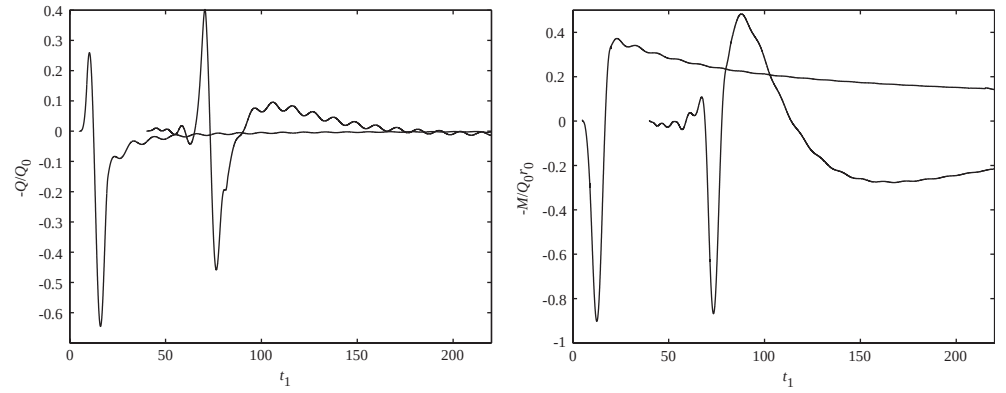

(a) The Shear force Q (b) The moment M

Fig. 4. Responses for BC2 at $x = 5$ and 40 with $\omega_0 = \pi/5$.

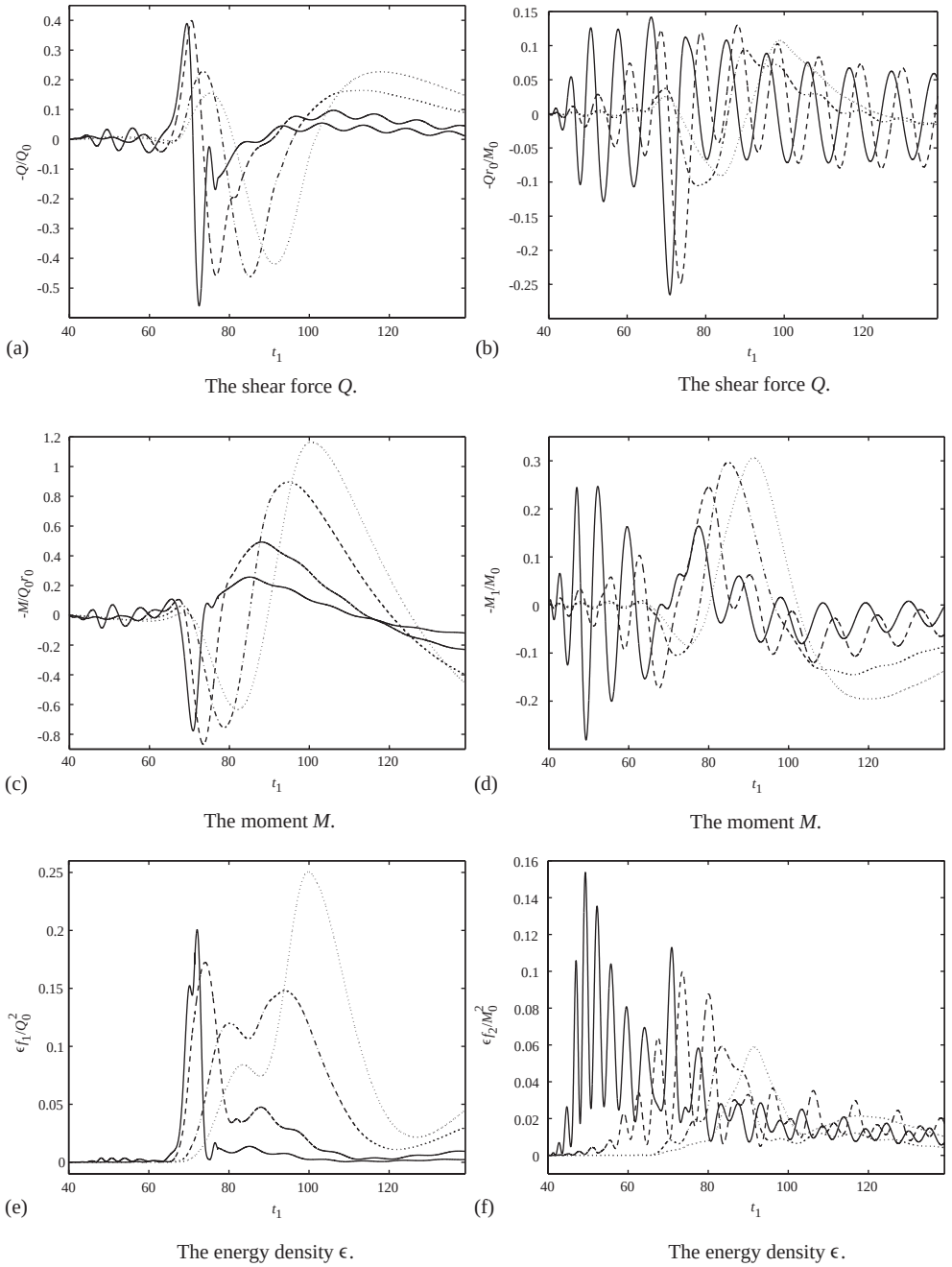

Fig. 5. Responses at $x = 40$ for the shear force, the moment and the energy density (first, second and third row, respectively) for BC2 and BC3 (left and right column, respectively). ——: $\omega_0 = 2\alpha_1$; - - - -: $\omega_0 = \alpha_1$; ·····: $\omega_0 = \alpha_1/2$; · · · · ·: $\omega_0 = \alpha_1/\sqrt{8}$.

time of the second wave front. In Fig. 3(c), this has been corrected by interpolating between the time-steps just before and after the arrival time of the second wave front. Note also, that the wave fields w and $\partial_x w$ are identical to the split fields w^+ and $\partial_x w^+$, since there are no waves propagating in the negative x direction. The split fields of the original wave splitting, $w_i^{\pm}$, would have been exponentially growing as e^t after the arrival of the second wave front.

It is also interesting to see the responses from an excitation with a somewhat more realistic pulse shape. In Fig. 4, the graphs, corresponding to Figs. 3(b)–(c), are presented for BC2 with $\omega_0 = \pi/5$. Here, the oscillating motion is not as pronounced as for the case of BC1, although the excitation contains the cut-off frequency.

For a better understanding of the influence of the frequency contents and the type of excitation, the responses at $x = 40$ for the shear force, the moment and the energy density were computed for four different values of ω_0, $\omega_0/\alpha_1 = 2, 1, 1/2, 1/\sqrt{8}$, for each of BC2 and BC3. The energy density $\varepsilon = \varepsilon_{pot} + \varepsilon_{kin}$ is given, with proper dimensions for all variables, by

$$\varepsilon_{pot} = \tfrac{1}{2}\left(\frac{f_1}{c_1^2}(\partial_t w)^2 + \frac{f_2}{c_2^2}(\partial_t \psi)^2\right),$$
$$\varepsilon_{kin} = \tfrac{1}{2}(f_1\gamma^2 + f_2(\partial_x \psi)^2). \tag{35}$$

The major part of the frequency contents of the excitation is below $\omega < 2\omega_0$ and, as is seen in Fig. 5, it is the responses for the two higher ω_0 that exhibit the oscillating behaviour and they also have a much larger part arriving before the second wave front, i.e., before $t_1 \approx 72$. Another striking feature is that, for these two values of ω_0, the responses from the different boundary conditions are very different. A much larger part of the energy arrives before the arrival of the second wave front for BC3, while, for the two lower values of ω_0, the responses are quite similar for both boundary conditions.

Hence, in order to obtain a strong signal in the time interval before the arrival of the second wave front, it is advantageous to excite the beam by an applied moment containing frequencies higher than α_3. Note however, the loss of accuracy of the Timoshenko theory for frequencies significantly higher than the cut-off frequency.

6. Concluding remarks

A purely directional wave splitting for the homogeneous Timoshenko beam has been derived. It has the advantages of giving split fields, transformation and Green's operator kernels, which do not grow exponentially in the time domain, as has been the problem with the original wave splitting [4]. However, for Green's operator kernels the problems with exponential behaviour and large cancellation effects are still present in the numerical evaluation of the kernels as can be seen from the integrals listed in Appendix B. With bounded split fields and operator kernels it is more feasible to propagate boundary data over large distances or for long time intervals. This is necessary when scattering problems are considered, where the measuring point is far from the scattering inhomogeneity or if the inhomogeneous region is large.

A consequence of deriving split fields other than those of the original wave splitting is that the dynamics of the split fields are no longer governed by a system of four first order one-way wave equations. For a homogeneous beam the split fields are governed by a decoupled system of two

second order one-way wave equations, see Eq. (15). If the beam is inhomogeneous, the system is coupled. Both systems may of course be written as coupled first order systems in terms of the split fields and they are obtained directly if the wave splitting transform, Eq. (21), is inserted into the original first order system. Depending on the nature of the inhomogeneity, different steps must be taken to account for the spatial dependence introduced by the inhomogeneity. However, the equations are no longer wave equations with explicit characteristics and this calls for some generalization of the time domain methods previously used in conjunction with the original wave splitting. Alternatively, one can use the purely directional wave splitting to propagate the wave fields to the boundary of an inhomogeneous region and then apply the original wave splitting in the inhomogeneous region if it is not too large.

Turning to the numerical results, the graphs display several interesting features, among them the oscillatory interaction between the shear and rotation angles, which is mainly the response from the thickness-shear mode. Moreover, the amount of propagated energy that arrives before the arrival of the second wave front depends largely on the type of excitation and on the frequency contents of the excitation. The knowledge of how to excite the beam in order to obtain a signal suitable for deconvolution may be valuable in the preparations of scattering experiments in the time domain.

Acknowledgements

This work has been supported by the Swedish Research Council for Engineering Sciences (TFR) and Swedish Research Council (VR). This is gratefully acknowledged. The author would also like to thank Prof. P. Olsson, Dr P.D. Folkow and Prof. A. Boström for enlightening discussions and useful suggestions.

Appendix A. Inverse transformation of $\tilde{\mathscr{A}}$

Here, the time-domain representation of $\tilde{\mathscr{A}}$ is obtained by approximate methods. It serves as an example of how to obtain time-domain representations for other operators or transformation matrix elements in this paper. For large s, the asymptotic expansion of $\tilde{\mathscr{A}}$ may be written as

$$\tilde{\mathscr{A}} - k_{1,\mathscr{A}} s = \tilde{K}_{\mathscr{A}}(s) \sim \sum_{k=1}^{\infty} a_k (k-1)! s^{-k}, \tag{A.1}$$

where $k_{1,\mathscr{A}} = \alpha_1^{-1} + \alpha_2^{-1}$. By the converse of Watson's Lemma [16], the asymptotic expansion of $\mathscr{A}$ for small t is

$$\begin{aligned} \mathscr{A} - k_{1,\mathscr{A}} \partial_t &= K_{\mathscr{A}}(\cdot) *, \\ K_{\mathscr{A}}(t) &\sim \mathrm{H}(t) \sum_{k=1}^{\infty} a_k t^{\,k-1}, \end{aligned} \tag{A.2}$$

where the convolution is defined as in Eq. (23). An asymptotic expansion of $K_{\mathscr{A}}$ for large values of t is obtained through contour integration of an approximation of $\tilde{K}_{\mathscr{A}}$. The branch cuts for $\tilde{K}_{\mathscr{A}}$

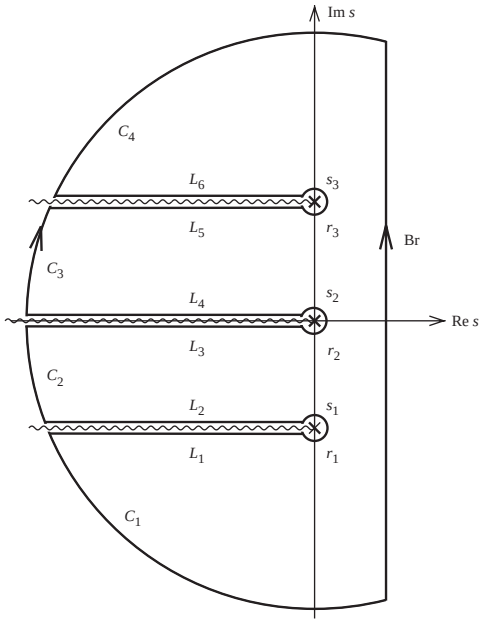

Fig. 6. Integration contours for asymptotic expansions.

(and $\mathscr{A}$) are drawn according to Fig. 6. The integral along the Bromwich contour is equivalent to the integral along the contour $C_1 + L_1 + \cdots + L_6 + C_7$. In this case the contribution from the integrals along $r_1, r_2, r_3, C_1, C_2, C_3, C_4$ is zero, which is not demonstrated here. In the neighbourhood of the branch points, $s = s_l$, $l = 1, 2, 3$, $\tilde{K}_{\mathscr{A}}$ is expanded in power series,

$$\tilde{K}_{\mathscr{A}}(s) = \sum_{k=0}^{\infty} b_{lk}(s - s_l)^{1/2+k} + \sum_{k=0}^{\infty} c_{lk}(s - s_l)^{k}. \tag{A.3}$$

The integrals along $L_1 + L_2$, $L_3 + L_4$ and $L_5 + L_6$ are approximated with the termwise integrals of the corresponding series expressions. Their sum is the approximation of $K_{\mathscr{A}}$ for large t,

$$K_{\mathscr{A}}(t) \sim \sum_{l=1}^{3} \mathrm{e}^{s_l t} \left(\sum_{k=0}^{\infty} \frac{b_{lk}}{\Gamma(-(k+1/2))} t^{-(k+3/2)} \right). \tag{A.4}$$

This technique can be studied in several textbooks, for example Ref. [17]. The short and long time behaviours are plotted in Fig. 7 for different truncations of the series expressions. As is seen, a region where the short and long time expansions overlap can be established.

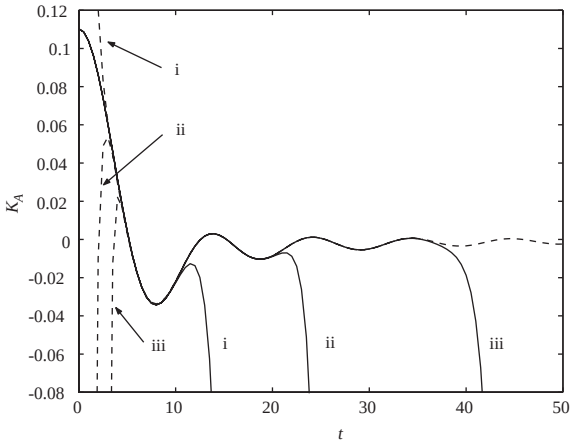

Fig. 7. Short time expansions (solid i–iii), with $2, 4, 8$ terms respectively, and long time expansions (dashed i–iii), with $16, 32, 64$ terms, respectively, for $K_{\mathscr{A}}$.

Appendix B. Integrals for numerical integration

The integrals I_1 through I_{12} are written in terms of

$$r = \frac{\sqrt{\alpha_1^2 + \eta^2}}{q\alpha_1}, \quad \theta_1 = \sqrt{\frac{q\eta(r+\eta)}{2\alpha_2}}, \quad \theta_2 = \sqrt{\frac{q\eta(r-\eta)}{2\alpha_2}}, \quad \theta_3 = \sqrt{\frac{q\eta + \sqrt{1+\eta^2}}{\alpha_2}},$$
$$\theta_4 = \frac{\sqrt{\alpha_1^2 - \eta^2}}{\alpha_1\alpha_2\theta_3}, \quad \theta_5 = \frac{q(r+\eta)}{\sqrt{1+\eta}}, \quad \theta_6 = \sqrt{\frac{2\alpha_2 q(r+\eta)}{1+\eta}}, \tag{B.1}$$

such that

$$I_1 = -2\pi^{-1}\int_0^{\alpha_1} \frac{\theta_3}{\theta_3^2+\theta_4^2}\left(\theta_4\cosh(x\eta^{1/2}\theta_4)\sin(\eta t) - \theta_3\sinh(x\eta^{1/2}\theta_4)\cos(\eta t)\right)\mathrm{d}\eta,$$

$$I_2 = \pi^{-1}\int_0^1 \left(\frac{\theta_5}{\sqrt{1-\eta}}\sinh(x\theta_1 - \eta t)\cos(x\theta_2) + \cosh(x\theta_1 - \eta t)\sin(x\theta_2)\right)\mathrm{d}\eta,$$

$$I_3 = 2\pi^{-1}\int_0^{\alpha_1} \frac{\theta_3\theta_4}{\theta_3^2+\theta_4^2}\sin(x\eta^{1/2}\theta_3 - \eta t)\,\mathrm{d}\eta,$$

$$I_4 = -2\pi^{-1}\int_0^{\alpha_1} \frac{1}{\theta_3^2+\theta_4^2}\left(\theta_3\sinh(x\eta^{1/2}\theta_4)\sin(\eta t) + \theta_4\cosh(x\eta^{1/2}\theta_4)\cos(\eta t)\right)\frac{\mathrm{d}\eta}{\sqrt{\eta}},$$

$$I_5 = \pi^{-1}\int_0^1 \theta_6\cosh(x\theta_1 - \eta t)\cos(x\theta_2)\frac{\mathrm{d}\eta}{\sqrt{\eta(1-\eta)}},$$

$$I_6 = 2\pi^{-1}\int_0^{\alpha_1} \frac{\theta_4}{\theta_3^2+\theta_4^2}\cos(x\eta^{1/2}\theta_3 - \eta t)\frac{\mathrm{d}\eta}{\sqrt{\eta}},$$

$$I_7 = 2\pi^{-1}\int_0^{\alpha_1} \frac{\theta_3\theta_4}{\theta_3^2+\theta_4^2}(\theta_3\cosh(x\eta^{1/2}\theta_4)\cos(\eta t) - \theta_4\sinh(x\eta^{1/2}\theta_4)\sin(\eta t))\sqrt{\eta}\,\mathrm{d}\eta,$$

$$I_8 = -\pi^{-1}\int_0^1 \theta_6(\theta_1^2+\theta_2^2)\cosh(x\theta_1-\eta t)\cos(x\theta_2)\frac{\mathrm{d}\eta}{\sqrt{\eta(1-\eta)}},$$

$$I_9 = 2\pi^{-1}\int_0^{\alpha_1} \frac{\theta_3^2\theta_4}{\theta_3^2+\theta_4^2}\cos(x\eta^{1/2}\theta_3-\eta t)\sqrt{\eta}\,\mathrm{d}\eta,$$

$$I_{10} = -2\pi^{-1}\int_0^{\alpha_1} \frac{\theta_4}{\theta_3^2+\theta_4^2}(\theta_4\sinh(x\eta^{1/2}\theta_4)\cos(\eta t) + \theta_3\cosh(x\eta^{1/2}\theta_4)\sin(\eta t))\,\mathrm{d}\eta,$$

$$I_{11} = \pi^{-1}\int_0^1 \left(\frac{\theta_5}{\sqrt{1-\eta}}\sinh(x\theta_1-\eta t)\cos(x\theta_2) - \cosh(x\theta_1-\eta t)\sin(x\theta_2)\right)\mathrm{d}\eta,$$

$$I_{12} = -2\pi^{-1}\int_0^{\alpha_1} \frac{\theta_3\theta_4}{\theta_3^2+\theta_4^2}\sin(x\eta^{1/2}\theta_3-\eta t)\,\mathrm{d}\eta.$$

The evaluation of these integrals is not straightforward. Besides being singular and oscillating integrals, it is also at this stage that the problems with exponentially growing kernels and large cancellation effects reappear, as several integrands contain hyperbolic trigonometric functions. It seems that the exponential behaviour is more critical than the oscillations. The singularities are found at the endpoints of the integration interval and can be handled by using a matching quadrature rule. For I_5 and I_8, Gauss–Chebyshev quadrature was used, for I_4, I_6 and the first term of I_2 and I_{11}, Gauss–Jacobi quadrature was used. The remaining integrals were computed with Gauss–Legendre quadrature.

Appendix C. Notes on some series representations

In Ref. [4] the eigenoperators λ_i, $i = 1, 2$, are represented in the time domain as

$$\lambda_i u(t) = c^{-1}\partial_t u(t) + (F_i(\cdot) * u(\cdot))(t), \tag{C.1}$$

where the convolution kernel functions $F_i(t)$ are exponentially growing. Time domain expressions for these functions are obtained as series expansions in the same way as described in Appendix A. For the asymptotic expansion for large time t however, only the contribution from the rightmost branch point is accounted for, since this contribution is exponentially larger than the contributions from the branch points on the imaginary axis. Thus all terms in the expansions are exponentially growing, more specifically, $F_i(t) = \mathcal{O}(t^{-3/2}\mathrm{e}^{t/\tau})$, $i = 1, 2$, as $t \to \infty$.

In view of the argument in Section 3.1, $F_1(t) + F_2(t) = \mathcal{O}(1)$. Therefore, the sum of the asymptotic series expansions in [4] must equal zero, which is seen by noting from Eq. (8) that $c_1(q+1)^{1/2} = c_2(q-1)^{1/2}$, for the terms presented. The series thus just differs by sign.

The exponentially growing behaviour of the split fields cancels when the physical fields are formed. Hence, the exponentially small contributions from the branch points on the imaginary

axis must be included to get accurate results of the physical fields for large values of the time variable.

References

[1] J.P. Corones, M.E. Davison, R.J. Krueger, Direct and inverse scattering in the time domain via invariant imbedding equations, *Journal of Acoustical Society of America* 74 (5) (1983) 1535–1541.
[2] R.J. Krueger, R.L. Ochs Jr., A Green's function approach to the determination of internal fields, *Wave Motion* 11 (1989) 525–543.
[3] A. Karlsson, Wave propagators for transient waves in one-dimensional media, *Wave Motion* 24 (1996) 85–99.
[4] P. Olsson, G. Kristensson, Wave splitting of the Timoshenko beam equation in the time domain, *Zeitschrift für Angewandte Mathematik und Physik* 45 (1994) 866–881.
[5] D.V.J. Billger, P.D. Folkow, The imbedding equations for the Timoshenko beam, *Journal of Sound and Vibration* 209 (4) (1998) 609–634.
[6] D.V.J. Billger, D.J.N. Wall, A time domain algorithm for the reflection of waves on a viscoelastically supported Timoshenko beam, *The Quarterly Journal of Mechanics and Applied Mathematics* 52 (1999) 211–236.
[7] P.D. Folkow, Time domain inversion of a viscoelastically restrained Timoshenko beam, *Inverse Problems* 15 (2) (1999) 551–562.
[8] D.V.J. Billger, P.D. Folkow, Wave propagators for the Timoshenko beam, *Wave Motion* 37 (4) (2003) 313–332.
[9] P.D. Folkow, G. Kristensson, P. Olsson, Time domain Green functions for the homogeneous Timoshenko beam, *The Quarterly Journal of Mechanics and Applied Mathematics* 51 (1) (1998) 125–141.
[10] D.V.J. Billger, Scattering of transient waves on a Timoshenko beam with varying cross section, Technical Report 1, Department of Mechanics, Chalmers University of Technology, 1998.
[11] D.V.J. Billger, Reconstruction of a varying cross section, Technical Report 3, Department of Mechanics, Chalmers University of Technology, 1998.
[12] S.P. Timoshenko, On the correction for shear of the differential equation for transverse vibrations of prismatic bars, *Philosophical Magazine* XLI (1921) 744–746 (reprinted in *The Collected Papers of Stephen P. Timoshenko*, McGraw-Hill, London, 1953).
[13] B.A. Boley, C.C. Chao, Some solutions of the Timoshenko beam equation, *Journal of Applied Mechanics* 22 (8) (1955) 579–586.
[14] K.F. Graff, *Wave Motion in Elastic Solids*, Oxford University Press, Oxford, 1975.
[15] D.G. Duffy, *Transform Methods for Solving Partial Differential Equations*, CRC Press, Boca Raton, FL, 1994.
[16] R. Wong, *Asymptotic Approximations of Integrals, Computer Science and Scientific Computing*, Academic Press, New York, 1989.
[17] J. Miklowitz, *The Theory of Elastic Waves and Waveguides*, 2nd Edition, North-Holland, Amsterdam, 1978.